Extraction of Design Characteristics of Multiobjective Optimization - Its Application to Design of Artificial Satellite Heat Pipe

Min Joong Jeong[1], Takashi Kobayashi[2], and Shinobu Yoshimura[3]

[1] Computational Biology Research Center, National Institute of Advanced Industrial Science and Technology, 2-43 Aomi, Koto-ku, Tokyo, 135-0064 Japan
jeong@cbrc.jp,
WWW home page: http://www.cbrc.jp
[2] Design Systems Engineering Center, Mitsubishi Electric Corp., 5-1-1 Ofuna, Kamakura, Kanagawa, 247-8501 Japan
[3] Institute of Environmental Studies, The University of Tokyo, 7-3-1 Hongo, Bunkyo-ku, Tokyo, 113-8656 Japan

Abstract. An artificial satellite design requires severe design objectives such as performance, reliability, weight, robustness, cost, and so on. To solve the conflicted requirements at the same time, multiobjective optimization is getting more popular in the design. Using the optimization, it becomes ordinary to get many solutions, such as Pareto solutions, quasi-Pareto solutions, and feasible solutions. The alternative solutions, however, are very difficult to be adopted to practical engineering decision directly. Therefore, to make the decision, proper information about the solutions in a function, parameter and real design space should be provided. In this paper, a new approach for the interpretation of Pareto solutions is proposed based on multidimensional visualization and clustering. The proposed method is applied to a thermal robustness and mass optimization problem of heat pipe shape design for an artificial satellite. The information gleaned from the propose approach can support the engineering decision for the design of artificial satellite heat pipe.

1 Introduction

A multiobjective optimization yields ideally innumerable alternative solutions known as Pareto solutions. There is no any superior one in the solutions because of their definition. However it is a very difficult task to judge Decision-Making (DM) from Pareto solutions. Two kinds of methods are well known to overcome the difficulty. First, preference methods give fixed preferences to objectives before multiobjective optimization, and then find one solution for DM. Second, trade-off methods are used to make DM from Pareto solutions after optimization. However, attempts to support DM with the preference or trade-off may result in poor design characters [1, 2]. That is because the DM using one solution may be inadequate when we include all factors that influence the choice of a particular design, such as durability and manufacturability. Therefore, if the whole set of

Pareto solutions are provided to engineers with proper information, they can use this information to choose the best overall design.

Visualization has been one of the most useful tools to guide information of correlations and characters between parameters, functions, and actual design shapes [3]. However, Pareto solutions are normally in a multidimensional space, and deter from extracting the information. To overcome this difficulty, the authors propose a synchronous 3D visualization. In the visualization, a multidimensional parameter and function space is divided into several 2D or 3D subspaces, and visualized in parallel. Each datum corresponds to a line segment between the subspaces and its shape in the real design space at the same time. Therefore, engineers can understand the correlation and effect of each datum in optimized solutions.

Furthermore, it is introduced that a clustering approach which considers a set of Pareto solutions as a group of several distinct clusters. This approach is based on the concept that the solutions consist of obvious characters in their function and parameter space. To measure the similarity and dissimilarity of solutions more essentially, the Euclidean distance and a point symmetry distance[4, 5] are hybrided.

As a practical engineering application, the proposed approach for interpretation of multiobjective solutions is applied to a thermal robustness and mass optimization problem of heat pipe shape for an artificial satellite [6]. Two functions and five parameters are considered in the design optimization. Using the proposed approach, we search for the information that can support engineering decision for the design of artificial satellite heat pipe.

2 Multiobjective Optimization of Artificial Satellite Heat Pipe

For a cooling system of artificial satellite, heat pipes based isothermal radiator panels are generally employed. Fin efficiency is dramatically improved using orthogonal interconnected (matrix layout) heat pipes as shown in Fig. 1. To maximize the fin efficiency of isothermal panels, the minimization of the temperature gradient between the lateral and header heat pipes becomes a very important design object [7]. On the other hand, saving the total mass (weight) of a thermal control subsystem is highly important to reduce load (pay load cost) on a booster-rocket. The satellite panels contain many embedded aluminum heat pipes, which generally occupy over 50% of the total mass of the fundamental radiator panels. Thus the thermal design of artificial satellite requires both the fin efficiency and mass saving of the heat pipes at the same time. Additionally, the operating temperature of the heat pipes is very widely ranging from $-20.0°C$ to $60.0°C$ in orbit. The thermal performance of the heat pipes must be stable in the temperature change. Therefore, the temperature dependency must be also taken into account for the heat pipe design. In this study, a combination of Response Surface Methodology (RSM) and Monte Carlo simulation is applied at first to formulate functions of the mass and thermal performance of the pipe

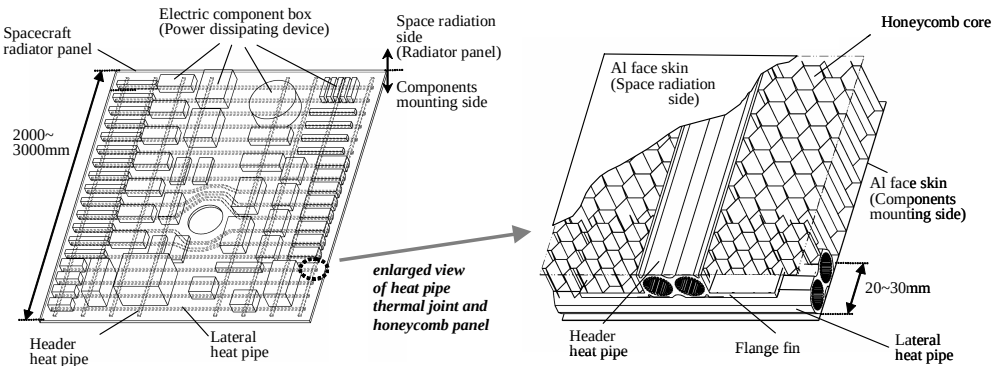

Fig. 1. Layout of heat pipes for satellite radiator.

structure [8, 10]. Here shape parameters of the heat pipes embedded within a satellite panel are design parameters, while the both of the mass and thermal robustness of the heat pipes are objective functions.

Table 1. Design parameter bounds.

Parameter	Lower Bound	Upper Bound
L_f	10.0mm	25.4mm
L_c	1.5mm	2.5mm
t_f	1.0mm	1.7mm

The design parameters determined by the mechanical designers are as follows: (i) length of fin (L_f), (ii) cutting length of adhesive attached area (L_c) and (iii) thickness of fin (t_f). These are illustrated in Fig. 2. Allowable ranges of the design parameters are given in Table 1. (iv) Adhesive thickness (t_b) and (v) operation temperature (T_{op}) are uncontrollable by the mechanical designers but affect the thermal performance of the heat pipes. The lateral and header heat pipes are bonded together by flange fin area with conductive epoxy. The adhesive thickness t_b has production tolerance, which influences the thermal performance of the heat pipes. To take account of this effect, it is assumed that the adhesive thickness has statistical normal distribution ranging from 0.12mm

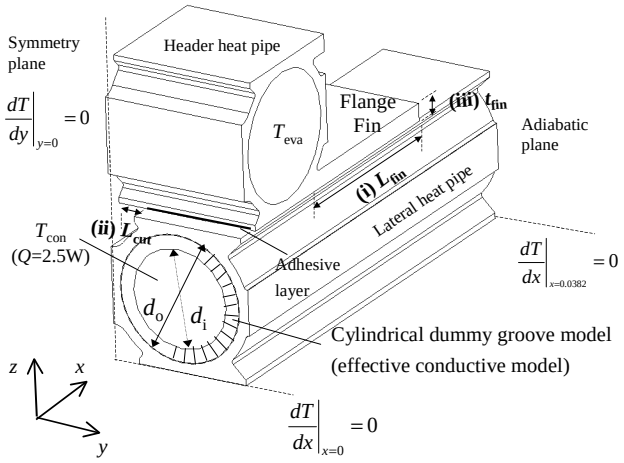

Fig. 2. Design parameters in 3D FE analysis model of heat pipes.

to 0.22mm. The operating temperature (T_{op}) for the heat pipes is required to range from -20.0°C to 60.0°C. The temperature dependency of heat transfer coefficient between evaporator and condenser at the inner wall of each heat pipe cannot be negligible from the view point of the stability of thermal performance. Consequently, these uncertain (uncontrollable) design parameters, t_b and T_{op}, are regarded as robust parameters. Their ranges are assumed as in Table 2. The three level experimental design [8–11] for the 5 design parameters which results in 27 analysis points was applied to selecting combinations of the analysis parameters to minimize the total number of finite element analyses.

Table 2. Uncertain design parameters.

Parameter	t_b	T_{op}
Lower Bound	0.12mm	-20.0°C
Upper Bound	0.22mm	60.0°C
Probability Distribution	Normal Distribution μ=0.17, σ=0.016	Normal Distribution μ=20.0, σ=14.3

2.1 Generation of Fitted Estimation Equations

27 Finite element analyses were performed to calculate the thermal performance of the parametric combinations which were given from the Taguchi orthogonal array - L27 [8, 9]. Those results were used to construct estimation equations for characteristic values G and M. Chebyshev's equation was considered to correlate the regression coefficients in multiple linear regression models. The calculated value G is the thermal conductance across the thermal joint of the heat pipes, defined as:

$$G = \frac{Q}{T_{con} - T_{eva}} \tag{1}$$

where T_{con} is the condensing liquid temperature in the lateral heat pipe, T_{eva} is the evaporating vapor temperature in the header heat pipe, and Q is the assumed quantity of the transported heat of 2.5W per a thermal joint. The determined response surface equation of G is as follows:

$$\begin{aligned}\hat{G} = f(L_f, L_c, t_f, t_b, T_{op}) &= 0.3745378 - 0.9352909t_b \\ &+1.01612{t_b}^2 + 2.324128e^{-2}L_c - 7.209993e^{-3}{L_c}^2 \\ &+l.838379e^{-3}L_f - 5.379707e^{-5}{L_f}^2 + 2.447391e^{-2}t_f \\ &+2.304583e^{-3}{t_f}^2 - 6.483411e^{-4}T_{op} - 9.232971e^{-7}{T_{op}}^2 \\ &-2.259702e^{-2}t_bL_c - 4.735652e^{-3}t_b{L_c}^2 + 0.1102442{t_b}^2L_c \\ &-9.702533e^{-3}{t_b}^2{L_c}^2 + 5.382211e^{-3}t_bL_f - 9.540484e^{-5}t_b{L_f}^2 \\ &+5.15048e^{-3}{t_b}^2L_f - 1.232524e^{-4}{t_b}^2{L_f}^2 + 0.2972589t_bt_f \\ &-0.1052935t_b{t_f}^2 - 0.5422262{t_b}^2t_f - 0.1829687{t_b}^2{t_f}^2\end{aligned} \tag{2}$$

The response surface equation for the total mass M also expressed in the following equation:

$$\begin{aligned}\hat{M} = f(L_f, L_c, t_f, t_b) &= (1313.877 - 75.5 * L_c + 11.0{L_c}^2 \\ &+1.402597L_f - 1.278314e^{-15}{L_f}^2 + 62.38776t_f \\ &-6.122449{t_f}^2 - 380.8t_b + 1120{t_b}^2) * 21;\end{aligned} \tag{3}$$

3 Multidimensional Pareto Solutions and Their Synchronous Visualization

To search the Pareto solutions of Eqs. 2 and 3, the Intermediate Tendency (IT) optimizer was used. Details of the optimizer described in Ref. [12, 13]. To put it briefly, the optimizer is a kind of genetic search algorithms, and consists of typical genetic operators such as fitness evaluation, selection, and mutation. To improve search efficiency, it adopts the IT recombination that is more robust in search ability than conventional intermediate recombination. In conventional recombination, such as the global intermediate recombination, any offspring individuals cannot deviate from d-dimensional search space covered by their parental individuals. In other word, if an optimum point is located out of the search space, any

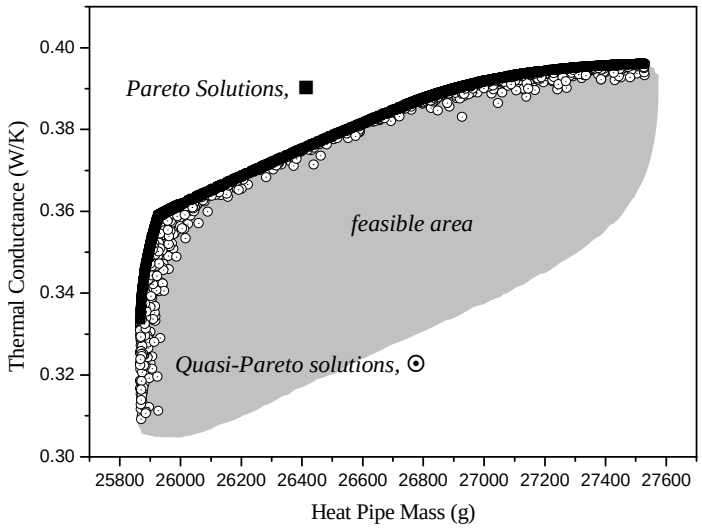

Fig. 3. Pareto solutions and quasi-Pareto solutions in function space.

offspring cannot reach the optimum point by the recombination. The IT recombination, however, yields offsprings depending on a discrepancy between parental individuals and randomly selected ones. The discrepancy is considered as the *tendency* in an evolution process, and the offsprings are yielded by adding the tendency to their parental individuals. Therefore the individuals of subsequent iteration are not bound to their parental search space. Superior performance of the IT recombination is shown in Ref. [12, 13].

For the multiobjective optimization, the optimizer is randomly changing preferences between the two objective functions and searches Pareto solutions in the function space. Figure 3 shows the Pareto solutions and also quasi-Pareto solutions, which were gathered during the optimization process. As shown in Fig. 3, there are many quasi-Pareto and Pareto solutions. Next it is explained how to search engineering information out of them.

3.1 Synchronous Visualization of Multidimensional Function and Parameter Spaces

Getting adequate information for determining a final solution is not an easy task especially if there are many Pareto solutions in a multidimensional space. Although parallel-coordinate methods [14, 15] handle multidimensional solutions, they have limitation in the number of solution sets and their amount of dimensions. To overcome the difficulty, a synchronous 3D visualization is proposed. Here, each of multidimensional parameter and function spaces is subdivided into several 2D or 3D subspaces, and visualized simultaneously. Each solution is

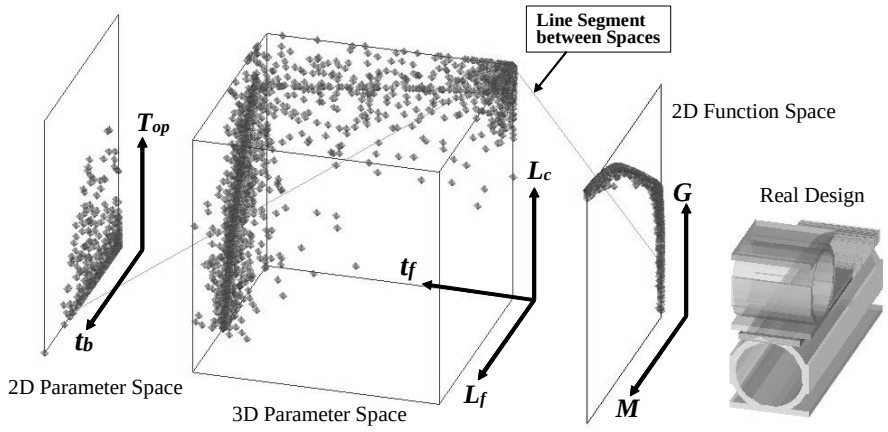

Fig. 4. Synchronous visualization of parameter subspaces, function space and real world design.

visualized in all the subspaces, and those corresponding points in the subspaces are connected by line segments. The real world space is also visualized at the same time. Through the interactive operation of the present visualization system, engineers can explore and understand the correlation among multidimensional function and parameter spaces and the real world space.

In the present heat pipe optimization, the 5-dimensional design parameter space is split to 2D and 3D subspaces, i.e., the 2D space of t_b and T_{op}, and the 3D space of L_f, L_c, and t_f, respectively. The 2D objective function space of $\hat{M}$ and $\hat{G}$ is remained as it is. The two parameter subspaces and the one function space are visualized simultaneously. Figure 4 shows the concept of the proposed visualization. The solutions in the original 7D space are separated into two parameter spaces and one function subspace. Moreover, a corresponding actual shape of the heat pipe is visualized with the subspaces. Corresponding points shown in different subspaces are connected by line segments. Therefore, it is easy to grasp the solution's correlation between the subspaces. The present visualization system was developed using the C language and the graphic-programming libraries named ADVENTURE AutoGL [16]. A programmable graphical user interface is also provided.

In Fig. 4, there are 3,552 quasi-Pareto solutions. It is clearly showed what kinds of parameter positions should make the optimum. For example, thin t_b and low T_{op} keep up the optimum. However, long L_f with small L_c and t_f does not correspond to the optimum. From this visualization, engineers can easily get ideas on parametric sensitivity of the present heat pipe shape design.

In addition, it can be interpreted the Pareto solutions. It is assessed the effects of t_b and T_{op} on the objective function space, i.e., of the mass and conductance

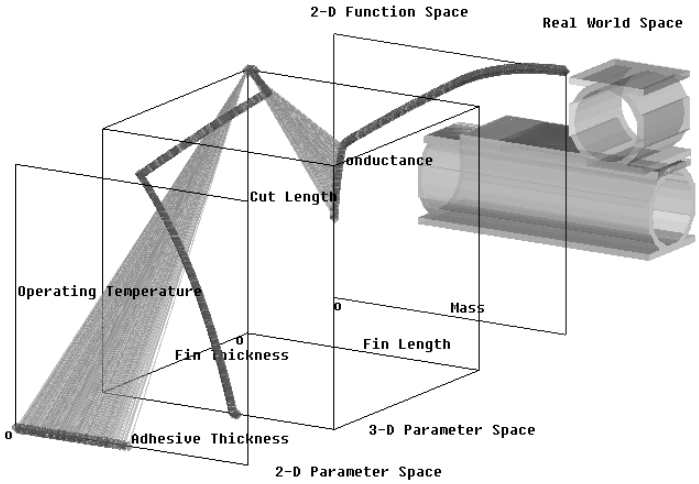

Fig. 5. Synchronous visualization of Pareto solutions of heat pipes.

in Fig. 5. In the figure, the line segments visualize the correlation among the subspaces. As shown in Fig. 5, the operating temperature is at its minimum, and only the variation of the adhesive thickness results in the changes of the objective functions $\hat{G}$ and $\hat{M}$. The three shape parameters L_f, L_c and t_f are almost tied up at the same point in their parameter subspace. Thus, without changing the shape parameter L_f, L_c and t_f, the design of heat pipes adopting thinner adhesive at lower operating temperature is expected to minimize the mass and to maximize the heat conductance. However, it is very difficult to change the operating temperature because of the design limitation of an orbit and thermal control system. Moreover, controls over the thickness of adhesive involve great uncertainty in manufacturing. To improve heat pipe performance, therefore, it is required to focus on the correlation of the shape parameters and the objective functions. For this purpose, the equations of $\hat{G}$ and $\hat{M}$ are regenerated to consider uncertainty of t_b and T_{op}. That is, the equations consist of only the three shape parameters, while t_b and T_{op} are taken into account as probability distributions as in Table 2.

3.2 Estimation Equations Considering Uncertain Parameters

The adhesive thickness t_b is assumed to be composed of random values with the normal distribution of $\mu_{t_b} = 170.0\mu$m and $\sigma_{t_b} = 16.7\mu$m. The operating temperature T_{op} is also assumed to be composed of random values with $\mu_{T_{op}} =$ 20.0K and $\sigma_{T_{op}} = 14.3$K. A direct sampling Monte Carlo simulation with the Box-Muller method is used to take into account random 2D parameters of the adhesive thickness t_b and the operating temperature T_{op}. The number of samples

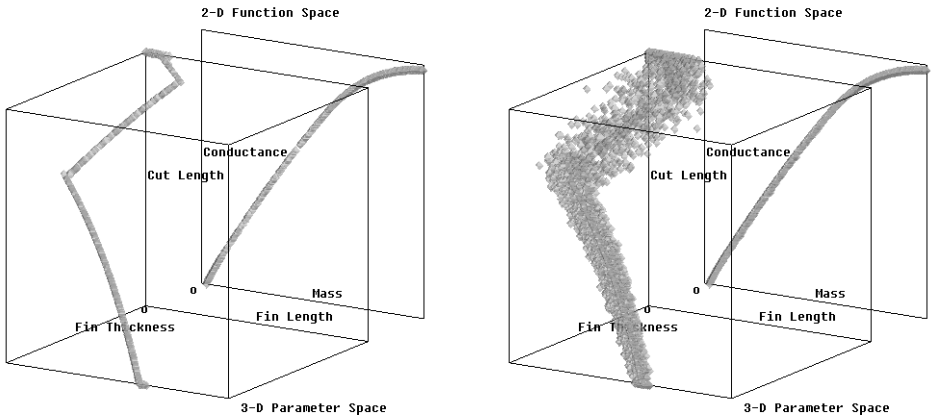

Fig. 6. Pareto (left) and quasi-Pareto (right) solutions of $\hat{\bar{G}}_R$ and $\hat{\bar{M}}_R$

for the Monte Carlo simulation is 1,000,000. An average thermal conductance, $\bar{G}_R$, under consideration of the thermal robustness is defined as follows:

$$\bar{G}_R = \int_{-20}^{60} \int_{0.12}^{0.22} G(t_b, T_{op}) \cdot f_p(t_b, T_{op}) dt_b dT_{op} \tag{4}$$

$$\cong \frac{1}{N} \sum_{m=1}^{1000} \sum_{n=1}^{1000} \hat{G}_R(t_{b,m}, T_{op,n}) \tag{5}$$

where $f_p(x)$ is a probability density function, and N is the total number of samples for Monte Carlo Simulation ($N = m * n = 1,000,000$).

The fitted polynominal equations for G and M, which consider the probability density of the uncontrollable parameters t_b and T_{op}, are regenerated using a quadratic model as:

$$\begin{aligned}\hat{\bar{G}}_R &= 2.261369e^{-2}L_c - 8.299937e^{-3}{L_c}^2 + 2.905449e^{-3}L_f \\ &-7.364545e^{-5}{L_f}^2 + 5.925684e^{-2}t_f - 1.028177e^{-2}{t_f}^2 \\ &+0.2312513\end{aligned} \tag{6}$$

$$\begin{aligned}\hat{\bar{M}}_R &= (1283.375 + 1.402597L_f - 1.278314e^{-15}{L_f}^2 \\ &-75.5L_c + 11.0{L_c}^2 + 62.38776t_f - 6.122449{t_f}^2) * 21\end{aligned} \tag{7}$$

4 Clustering of Pareto Solutions

Figure 6 shows the Pareto and the quasi-Pareto solutions of $\hat{\bar{G}}_R$ and $\hat{\bar{M}}_R$. As shown in the figure, the Pareto solutions and the quasi-Pareto ones have almost

the same function values. However, the quasi-Pareto solutions have much more variance in the parameter space than the Pareto ones. In the engineering sense, such quasi-Pareto solutions with parametric variance also seem beneficial because of their increasing design freedom such as manufacturability. Therefore, both Pareto and quasi-Pareto solutions should be examined in more detail before making the final decision of the heat pipe design.

To do so, one of clustering algorithms is applied to the solutions. Overviews of clustering algorithms can be found in Ref. [13, 17, 19]. If the solutions are appropriately classified into several clusters, it is expected that engineers can interpret mathematical as well as engineering characteristics of the solutions in a more abstract manner.

The clustering function without fuzziness is

$$C_F{}'(X, U, V) = \sum_{k=1}^{K} \sum_{i=1}^{n} u_{ik} \cdot dis(\boldsymbol{x}_i, \boldsymbol{v}_k) \tag{8}$$

where $X = \{\boldsymbol{x}_1, \ldots, \boldsymbol{x}_n\} \subseteq \mathbb{R}^d$ is a set of n solutions in a d-dimensional real-valued space, n is the number of solutions to be clustered, K is the number of clusters, $u_{ik} \in \{0, 1\}$ is the membership of $\boldsymbol{x}_i$ belonging to the kth cluster, and $\boldsymbol{v}_k$ is the center of the kth cluster. $dis(\boldsymbol{x}_i, \boldsymbol{v}_k)$ means a distance between $\boldsymbol{x}_i$ and $\boldsymbol{v}_k$.

4.1 Point Symmetry Distance Measure

Many clustering algorithms are adapting the Minkowski [17] metric to measure dissimilarity, i.e., distance $dis(\boldsymbol{x}_i, \boldsymbol{v}_k)$, in the clustering function. The Minkowski metric for measuring the dissimilarity between a solution $\boldsymbol{x}_i = (x_{i1}, \cdots, x_{id})^T$ and a center (search vector) $\boldsymbol{v}_k = (v_{k1}, \cdots, v_{kd})^T$ is defined as:

$$d_{mink}(\boldsymbol{x}_i, \boldsymbol{v}_k) = [\sum_{j=1}^{d} |x_{ij} - v_{kj}|^r]^{1/r} \tag{9}$$

where $r \geq 1$. The three common Minkowski metrics are illustrated in Fig. 7. The Euclidean distance ($r = 2$) is one of the most common Minkowski distance metrics. Conventional clustering algorithms with the Euclidean distance tend to detect hyperspherical-shaped clusters.

Since the distribution shapes of Pareto and quasi-Pareto solutions are much closer to combinations of hyperellipsoidal or hyperline shapes than hyperspherical shapes, the Euclidean distance measure may not be a good choice for searching the characteristics of the solutions. Instead, a point symmetry distance measure [18] is adopted. The distance measure is a more flexible to find clusters of hyperellipsoidal or hyperline shapes. Given n solutions, the point symmetry distance between a solution $\boldsymbol{x}_i$ and a cluster center $\boldsymbol{v}_k$ is defined as:

$$d_{sym}(\boldsymbol{x}_i, \boldsymbol{v}_k) = min_{\substack{p=1,\cdots,n \\ and \\ p \neq i}} \frac{||(\boldsymbol{x}_i - \boldsymbol{v}_k) + (\boldsymbol{x}_p - \boldsymbol{v}_k)||}{(||(\boldsymbol{x}_i - \boldsymbol{v}_k)|| + ||(\boldsymbol{x}_p - \boldsymbol{v}_k)||)} \tag{10}$$

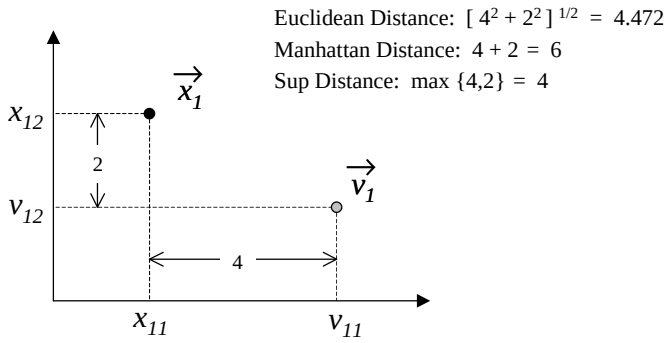

Fig. 7. Three common Minkowski metrics [17].

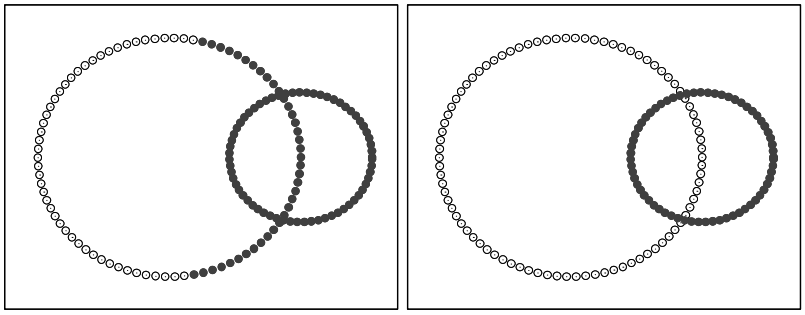

Fig. 8. Two clusters measured by the Euclidean distance (left) and point symmetry distance (right).

where the denominator term is used to normalize the point symmetry distance. Due to such normalization, the point symmetry distance becomes insensitive to the Euclidean distances $||(\boldsymbol{x}_i - \boldsymbol{v}_k)||$ and $||(\boldsymbol{x}_p - \boldsymbol{v}_k)||$.

Figure 8 shows different clustering results of sample patterns obtained by the two different distance measures. The clustering result obtained by the Euclidean distance shows quantitatively well separated two clusters. The result obtained by the point symmetry distance shows that each clustered pattern possesses the characteristic of its shape, i.e., a circle in this case. However a group of patterns is often composed of patterns have scarce symmetric similarity among them. Therefore, the Euclidean distance measure and the point symmetry distance measure are hybridized for the clustering function Eq. 8. The hybrid measure is as follows:

$$dis(\boldsymbol{x}_i, \boldsymbol{v}_k) = \begin{cases} \text{if } d_{sym}(\boldsymbol{x}_i, \boldsymbol{v}_k) > \theta, & d_{mink}(\boldsymbol{x}_i, \boldsymbol{v}_k), \ r = 2 \\ \text{else,} & d_{sym}(\boldsymbol{x}_i, \boldsymbol{v}_k) \end{cases} \tag{11}$$

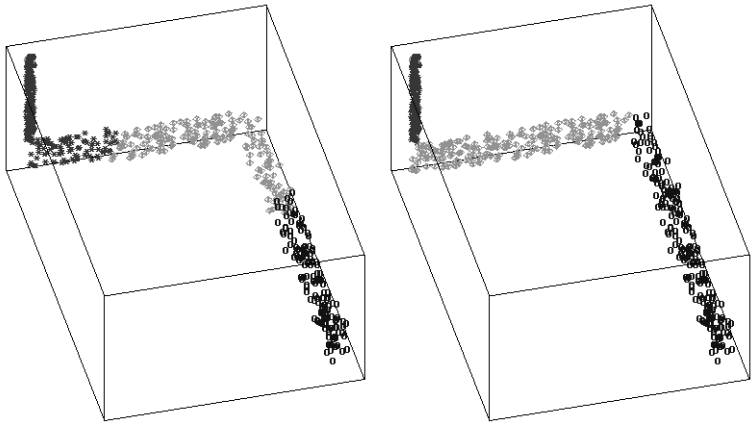

Fig. 9. Three clusters obtained by using the Euclidean distance (left) and point symmetry distance (right).

where θ is a tradeoff parameter between the two distance measures. Iterative clustering algorithms such as the K-means algorithm [17, 19] depend their results on initial centers employed. In the proposed clustering function, the clustering results severely vary with θ. To overcome those problems simultaneously, the hybrid distance measure is adapted to the evolutionary clustering algorithm [12]. In the minimization of the clustering function, the tradeoff parameter is predefined as a constant. Only the centers are considered as variables of the clustering function, and they are searched by evolutionary processes including selection, recombination, and mutation.

Figure 9 shows an example for verification of the proposed clustering algorithm. The patterns shown in the figure are generated by imitating Pareto solutions. The result by using the Euclidean distance shows three clusters separated each other in geometry only. However, the proposed measure makes the break surfaces between clusters when the flow of solutions' variation is changed. The result by using the point symmetry distance shows what kinds of parametric characteristics are transformed in a parameter space. It is confirmed by the comparison between both results in Fig. 9 that the proposed distance is better suited for gathering engineering information. Therefore, the proposed clustering is employed with the hybrid distance in the following section.

4.2 Cluster Interpretation of Multiobjective Pareto and Quasi-Pareto Solutions

The proposed clustering method was applied to 4,061 Pareto and quasi-Pareto solutions of Eq. 6 and 7. The solutions were clearly classified into two clusters

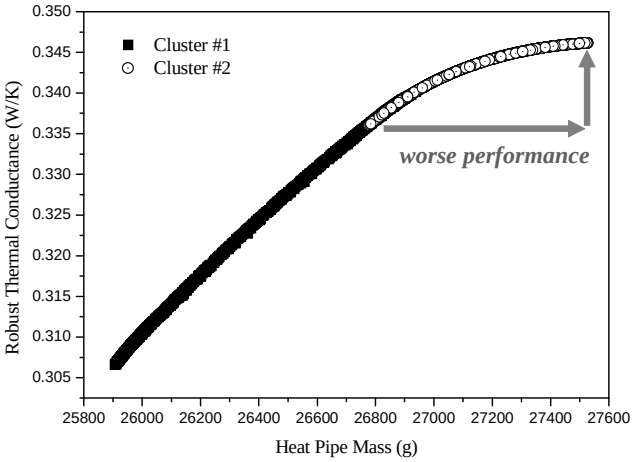

Fig. 10. Clustering in function space.

that have distinct parametric characteristics. One cluster #1 includes 1,993 solutions dominated mainly by the fin thickness and slightly by the cut length. The solutions in the cluster are not sensitive to the fin length. Cluster #2 has 2,068 solutions varying with the fin length and the cut length. In this case, the thickness of fins is fixed to its maximum value, 1.7mm. Figure 10 shows the projection of the two clusters in the parameter space onto the object function space. The figure clearly shows that the solutions in cluster #1 are in the range of increasing both thermal conductance and mass in a reasonable rate. On the other hand, the solutions in cluster #2 are in the range of increasing the mass exponentially. For example, the 63.6% possible increase of the mass raises the 84.8% of the possible thermal conductance in cluster #1. However, in cluster #2, the 46.9% of the mass increase makes only the 25.6% of the conductance. Thus the solutions in cluster #1 must be candidates for the best overall design on the view point of minimizing the mass and maximizing the conductance.

Figure 11 shows the clustering result in both of the function and parameter spaces. Since thick fins reduce heat resistance, the solutions in cluster #1 having thick fins increase the thermal conductance. In case of cluster #2 which has the solutions with long fins, however, the fin parts away from the pipe junction have very small heat flux. Therefore the ends of the long fins just enlarge the mass without increasing the conductance. Through such interpretation based on the proposed visualization and clustering, thermal designers can obtain useful information for their decision of final design. Especially, the solutions on the border between the two clusters are the most possible for DM when we focus on the maximization of the thermal conductance.

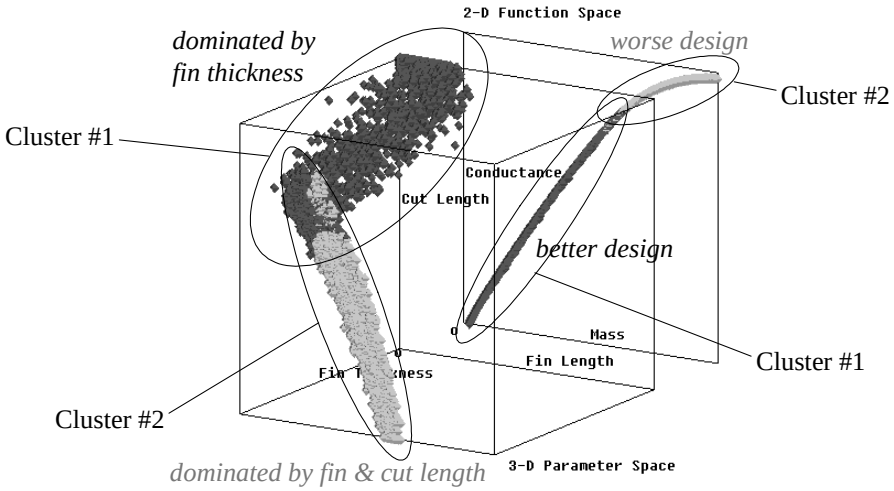

Fig. 11. Design parameters corresponding to optimum design.

4.3 Conclusions

In this paper, it was described a new procedure to interpret Pareto and quasi-Pareto solutions of multiobjective optimization. A synchronous 3D visualization was used to explore the structure and characteristics of multidimensional solutions. The visualization presents the correlations between a parameter, function, and actual design space in their subdivided spaces. Moreover, to make clusters of solutions in engineering meanings, we presented a clustering algorithm which has a hybrid distance measure of the Euclidean and point symmetry distance. The clustering algorithm shows similarity and dissimilarity among the solutions and beneficial information for designers.

As a practical engineering application, the proposed approach was applied to a multiobjective optimization of an artificial satellite. The design optimization has two functions, two uncontrollable parameters, and three shape parameters of heat pipes of the satellite. The synchronous visualization helps one to understand the design effect of each solution from the Pareto and quasi-Pareto solutions. The clustering of the optimization solutions guides the shape parameters those corresponds to worse or better design clearly. Through such interpretation based on the proposed visualization and clustering, the thermal designers can obtain useful information for their decision of final design.

References

1. Tappeta, R. V., Renaud, J. E.: Iterative multiobjective optimization procedure. AIAA Journal **37**, 7 (1999) 881–889

2. Tappeta, R. V., Renaud, J. E.: Iterative multiobjective optimization design strategy for decision based design. Journal of Mechanical Design, **123**, June (2001) 205–215
3. Meng, Z., Pao, Y. H.: Visualization and selforganization of multidimensional data through equalized orthogonal mapping. IEEE Transactions on Neural Networks **11**, 4 (2000) 1031–1038
4. Miller,W.: Symmetry Groups and Their Applications. (1972) Academic Press, London
5. Weyl, H.: Symmetry. (1952) Princeton University Press, Princeton, NJ
6. Kobayashi, T., Nomura, T., Kamifuji, M., Yao, A., Ogushi, T.: Thermal robustness and mass optimization of heat pipe shape for spacecraft panel using a combination of responce surface methodology and monte carlo simulation. Proceedings of 28th Design Automation Conference, (2002) DETC2002/DAC-34055
7. Kelly, W. H., Reisenweber, J. H.: Thermal performance of embedded heat pipe spacecraft radiator panels. SAE Technical Paper, (1993) 932158
8. Taguchi, G.: Design of Experiment. Japanese Standards Association, (1979) in Japanese
9. Taguchi, G., Konishi, S.: Orthogonal Arrays and Linear Graphs. ASI press, (1987) Dearborn, MI
10. Myers, R. H., Montegomery, D. C.: Responce Surface Methodology: Process and Product Optimization Using Design Experiments. (1995) Wiley Inter-Science
11. Kashiwamura, T., Shiratori, M.: Structural optimization using the design of experiments and mathematical programming. Transactions of the JSME **62**, 601 (1996) 208–223, in Japanese
12. Jeong, M. J., Yoshimura, S.: An evolutionary clustering approach to pareto solutions in multiobjective optimization. Proceedings of 28th Design Automation Conference, (2002) DETC2002/DAC-34048
13. Jeong, M. J.: Integrated Support System for Decision-Making in Design Optimization. PhD Thesis, (2003) The University of Tokyo
14. Chen, J. X.: Data visualization: Parallel coordinates and dimension reduction. Computing in Science and Engineering **3**, 5 (2001) 110–113
15. Inselberg, A.: Visulaiztion and data mining of highdimensional data. Chemometrics and Intelligent Laboratory Systems **60**, (2002) 147–159
16. Kawai, H.: Development of a 3-d graphics and gui tookit for making pre- and post-processing tools. Proceedings of the Conference on Computational Engineering and Science **8**, 2 (2003) 889–892, in Japanese
17. Jain, A. K., Dubes, R. C.: Algorithms for Clustering Data. Prentice-Hall, (1989) Englewood Cliffs, New Jersey
18. Su, M., Chou, C.: A modified version of the k-means algorithm with a distance based on cluster symmety. IEEE Trans. on Pattern Analysis and Machine Intelligence **23**, 6 (2001) 674–680
19. Mirkin, B.: Mathematical Classification and Clustering. Kluwer Academic Publishers, (1996) New York